Research Article | Vol. 26, No. 9 | 30 Apr 2018 | OPTICS EXPRESS 12081
Optics EXPRESS

Double-range near-infrared acetylene detection using a dual spot-ring Herriott cell (DSR-HC)

MING DONG,[1] CHUANTAO ZHENG,[1,2,*] DAN YAO,[1] GUOQIANG ZHONG,[1] SHUZHUO MIAO,[1] WEILIN YE,[2,3] YIDING WANG,[1] AND FRANK K. TITTEL[2]

[1]*State Key Laboratory of Integrated Optoelectronics, College of Electronic Science and Engineering, Jilin University, 2699 Qianjin Street, Changchun 130012, China*
[2]*Department of Electrical and Computer Engineering, Rice University, 6100 Main Street, Houston, Texas 77005, USA*
[3]*College of Engineering, Shantou University, 243 Daxue Road, Shantou 515063, China*
[*]*zhengchuantao@jlu.edu.cn*

Abstract: Design and fabrication of a dual spot-ring Herriott cell (DSR-HC) were proposed. The sealed Herriott cell with a dimensional size of 5.5 cm × 9.2 cm × 32.1 cm, possessed two input/output coupling holes leading to two absorption path lengths of ~20 m and ~6 m, respectively. An acetylene (C_2H_2) sensor system with a double-range was developed using the DSR-HC and wavelength modulation spectroscopy (WMS) technique. A near-infrared distributed feedback (DFB) laser was employed for targeting a C_2H_2 absorption line at 6521.2 cm^{-1}. C_2H_2 concentration measurements were carried out by modulating the laser at a 5 kHz frequency and demodulating the detector signal with LabVIEW software. An Allan-Werle deviation analysis indicated that the limit of detection (LoD) for the two absorption path lengths of 20 m and 6 m are 7.9 parts-per-million in volume (ppmv) and 4.0 ppmv, respectively. The DSR-HC concept can be used to fabricate similar cells for single-gas detection requiring two different detection ranges as well as for dual-gas detection requiring different absorption path lengths.

© 2018 Optical Society of America under the terms of the OSA Open Access Publishing Agreement

OCIS codes: (280.3420) Laser sensors; (300.6340) Spectroscopy, infrared; (140.5965) Semiconductor lasers, quantum cascade.

References and links

1. J. S. Li, G. Durry, J. Cousin, L. Joly, B. Parvitte, and V. Zeninari, "Self-broadening coefficients and positions of acetylene around 1.533 μm studied by high-resolution diode laser absorption spectrometry," J. Quant. Spectrosc. Radiat. Transf. **111**(15), 2332–2340 (2010).
2. Y. Cao, W. Jin, H. L. Ho, L. Qi, and Y. H. Yang, "Acetylene detection based on diode laser QEPAS: combined wavelength and residual amplitude modulation," Appl. Phys. B **109**(2), 359–366 (2012).
3. K. C. Utsav, E. F. Nasir, and A. Farooq, "A mid-infrared absorption diagnostic for acetylene detection," Appl. Phys. B **120**(2), 223–232 (2015).
4. G. M. Ma, S. J. Zhao, J. Jiang, H. T. Song, C. R. Li, Y. T. Luo, and H. Wu, "Tracing Acetylene Dissolved in Transformer Oil by Tunable Diode Laser Absorption Spectrum," Sci. Rep. **7**(1), 14961 (2017).
5. R. Ghorbani and F. M. Schmidt, "ICL-based TDLAS sensor for real-time breath gas analysis of carbon monoxide isotopes," Opt. Express **25**(11), 12743–12752 (2017).
6. C. G. Li, L. Dong, C. T. Zheng, and F. K. Tittel, "Compact TDLAS based optical sensor for ppb-level ethane detection by use of a 3.34 μm room-temperature CW interband cascade laser," Sens. Actuators B Chem. **232**, 188–194 (2016).
7. C. T. Zheng, W. L. Ye, N. P. Sanchez, C. G. Li, L. Dong, Y. D. Wang, E. J. Griffin, and F. K. Tittel, "Development and field deployment of a mid-infrared methane sensor without pressure control using interband cascade laser absorption spectroscopy," Sens. Actuators B Chem. **244**, 365–372 (2017).
8. N. Liu, H. Deng, T. He, Y. Liu, L. Zhang, and J. Li, "Measurements of new absorption lines of acetylene at 1.53μm using a tunable diode laser absorption spectrometer," Spectrochim. Acta A Mol. Biomol. Spectrosc. **186**, 1–7 (2017).
9. P. Kluczynski, M. Jahjah, L. Nähle, O. Axner, S. Belahsene, M. Fischer, J. Koeth, Y. Rouillard, J. Westberg, A. Vicet, and S. Lundqvist, "Detection of acetylene impurities in ethylene and polyethylene manufacturing processes using tunable diode laser spectroscopy in the 3-μm range," Appl. Phys. B **105**(2), 427–434 (2011).

#320642 https://doi.org/10.1364/OE.26.012081
Journal © 2018 Received 25 Jan 2018; revised 18 Apr 2018; accepted 22 Apr 2018; published 26 Apr 2018

Optics EXPRESS

10. F. Song, C. Zheng, W. Yan, W. Ye, Y. Wang, and F. K. Tittel, "Interband cascade laser based mid-infrared methane sensor system using a novel electrical-domain self-adaptive direct laser absorption spectroscopy (SA-DLAS)," Opt. Express **25**(25), 31876–31888 (2017).
11. Q. He, M. Lou, C. Zheng, W. Ye, Y. Wang, and F. K. Tittel, "Repetitively Mode-Locked Cavity-Enhanced Absorption Spectroscopy (RML-CEAS) for Near-Infrared Gas Sensing," Sensors (Basel) **17**(12), 2792 (2017).
12. J. B. McManus, P. L. Kebabian, and M. S. Zahniser, "Astigmatic mirror multipass absorption cells for long-path-length spectroscopy," Appl. Opt. **34**(18), 3336–3348 (1995).
13. D. Richter, A. Fried, B. P. Wert, J. G. Walega, and F. K. Tittel, "Development of a tunable mid-IR difference frequency laser source for highly sensitive airborne trace gas detection," Appl. Phys. B **75**(2-3), 281–288 (2002).
14. H. Moser, A. Genner, J. Ofner, C. Schwarzer, G. Strasser, and B. Lendl, "Application of a ring cavity surface emitting quantum cascade laser (RCSE-QCL) on the measurement of H_2S in a CH_4 matrix for process analytics," Opt. Express **24**(6), 6572–6585 (2016).
15. W. R. Trutna and R. L. Byer, "Multiple-pass Raman gain cell," Appl. Opt. **19**(2), 301–312 (1980).
16. S. M. Adler-Golden, N. Goldstein, F. Bien, M. W. Matthew, M. E. Gersh, W. K. Cheng, and F. W. Adams, "Laser Raman sensor for measurement of trace-hydrogen gas," Appl. Opt. **31**(6), 831–835 (1992).
17. J. A. Nwaboh, J. Hald, J. K. Lyngso, J. C. Petersen, and O. Werhahn, "Measurements of CO2, in a multipass cell and in a hollow-core photonic bandgap fiber at 2 μm," Appl. Phys. B **110**(2), 187–194 (2013).
18. D. McDermitt, G. Burba, L. Xu, T. Anderson, A. Komissarov, B. Riensche, J. Schedlbauer, G. Starr, D. Zona, W. Oechel, S. Oberbauer, and S. Hastings, "A new low-power, open-path instrument for measuring methane flux by eddy covariance," Appl. Phys. B **102**(2), 391–405 (2011).
19. A. Pogány, S. Wagner, O. Werhahn, and V. Ebert, "Development and metrological characterization of a tunable diode laser absorption spectroscopy (TDLAS) spectrometer for simultaneous absolute measurement of carbon dioxide and water vapor," Appl. Spectrosc. **69**(2), 257–268 (2015).
20. D. Herriott, H. Kogelnik, and R. Kompfner, "Off-Axis Paths in Spherical Mirror Interferometers," Appl. Opt. **3**(4), 523–526 (1964).
21. D. R. Herriott and H. J. Schulte, "Folded Optical Delay Lines," Appl. Opt. **4**(8), 883–889 (1965).
22. J. Altmann, R. Baumgart, and C. Weitkamp, "Two-mirror multipass absorption cell," Appl. Opt. **20**(6), 995–999 (1981).
23. J. B. McManus, P. L. Kebabian, and M. S. Zahniser, "Astigmatic mirror multipass absorption cells for long-path-length spectroscopy," Appl. Opt. **34**(18), 3336–3348 (1995).
24. G. S. Engel and E. J. Moyer, "Precise multipass Herriott cell design: derivation of controlling design equations," Opt. Lett. **32**(6), 704–706 (2007).
25. C. G. Tarsitano and C. R. Webster, "Multilaser Herriott cell for planetary tunable laser spectrometers," Appl. Opt. **46**(28), 6923–6935 (2007).
26. http://www.spectraplot.com/
27. J. Reid and D. Labrie, "Second-harmonic detection with tunable diode lasers — Comparison of experiment and theory," Appl. Phys. B **26**(3), 203–210 (1981).

1. Introduction

Acetylene (C_2H_2) is colorless, inflammable and explosive at ambient temperature and pressure and is widely used in the industrial field as a fuel and a basic raw material in organic synthesis. Accurate measurement and monitoring on C_2H_2 in the industrial field is therefore extremely important for assuring a high quality of raw petrochemical materials and products [1–4]. Tunable laser absorption spectroscopy (TDLAS) has been widely used in trace gas detection because of its non-intrusive, sensitive and selective sensing characteristics [5–7]. For example, based on TDLAS technique, both near- and mid-infrared sensor systems were proposed for C_2H_2 detection using a 76 m long-path absorption cell (AMAC-76, Aerodyne Research Inc) [8] and a 15 cm gas absorption cell [9].

A multi-pass gas cell [10] and a high-fineness cavity [11] are two kinds of gas absorption approaches for enhancing sensitivity based on different principles, which are widely used in TDLAS based gas sensor systems. A multi-pass cell realized by symmetric spherical mirrors in a Herriott cell configuration is commonly used for trace-gas detection [12–14], in Raman spectroscopy [15-16] and atmospheric *in situ* instrumentation [17–19]. There are many types of ray-trace optical models that can result in multiple reflections such as the Herriott White or Chernin cell. The Herriott cell was proposed by D.R. Herriott [20-21] in 1964. The cell consisted of two equal and coaxial mirrors, and the distribution of spots and reentrant condition were discussed in [20, 21]. In 1981, J. Altmann established that the beam exited a Herriott cell with a fixed direction regardless of the path length and that the angular alignment of the mirrors and spacing are not critical [22]. In 1995, McManus [23] reported that the

Optics EXPRESS

distribution of spots using mirrors with different radii with an effective adjustability by rotating the mirror. In 2007, G.S. Engel derived the design equations for exact solutions to the Herriott cell problem of approximate dimensions and imperfect patterns [24]. C.G. Tarsitano presented a four-channel Herriott cell configuration for a specific application as the sample cell of a tunable laser spectrometer instrument [25]. The current development trend of a Herriott cell is to change its mode pattern from a single-ring to multi-rings and to change the structure from a two-dimensional plane to a three-dimensional space.

The detection range and sensitivity are the critical parameters of an infrared spectroscopic gas sensor. The detection range of a gas sensor with a certain absorption path length is usually limited to 2-3 orders of magnitude in concentration levels. For example, a ppb level gas sensor cannot detect a gas concentration level of a few hundred parts-per-million in volume (ppmv) or higher because of a too strong gas absorption. For a highly-sensitive sensor, a target gas with a relatively high concentration has to be diluted before measurement, which limits the application of a gas sensor. In order to address this problem, modeling and a new design of a dual spot-ring Herriott cell (DSR-HC) is proposed, which has two independent entrance holes leading to two different absorption path lengths. The Herriott cell was fabricated and sealed based on the design parameters and C_2H_2 detection experiments were carried out to validate the DSR-HC performance. The proposed Herriott cell model can also be used to fabricate similar cells with different dual absorption lengths. Besides the detection of one single gas species with two different detection ranges, such a gas cell can also be adopted in dual-gas detection requiring different absorption lengths for a specific sensitivity.

2. Design of the DSR-HC

2.1. DSR-HC model and simulation

A generic model of a DSR-HC was developed based on MATLAB and shown in Fig. 1(a). There are two entrance-holes (EH1, EH2) on mirror A and two rays enter and emit the DSR-HC through the same entrance hole, respectively. In this way, two light paths were obtained. Generally, the size of a Herriott cell is determined by the actual requirements, including the distance between the mirrors and the mirror radius. The number of reflections can be increased to obtain a relative long light path. There are two ways to increase the number of reflections. Firstly, the size of the exit hole should be small in order to minimize the output of reflected ray from the cell; Secondly, the distribution of the reflected spots should be close to the edge of the mirror in order to accommodate more reflected spots. However, more reflections mean more attenuation of the light intensity due to the limited mirror reflectivity, which decreases the signal-noise ratio (SNR).

A large number of reflections will increase reflected spots density on the mirrors. When a reflected spot is near the entrance hole with a relatively large radius, there is a possibility that part of light leak from the cell through the entrance hole and reach the detector during the reflections. In this case, the measured light path is equal to the light path corresponding to the reflection order of the leaked spot, thereby causing an error between the measured light path and the designed light path. Therefore, the shape of the spots distribution must be adjustable and the radius of the incident spot has to be limited to avoid light leakage.

As shown in Fig. 1(b), the direction vector of the incident ray was normalized to (1, v, w). The spot distributions in different colors correspond to different values of v, where w = 0.0379. The elliptical outline of the spots distribution rotates forward as v increases. There is a special position (marked with red dots) where the short axis of the fitting ellipse is parallel to the x-axis and the long axis of the fitting ellipse is parallel to the y-axis. As shown in Fig. 1(c), the spot distributions in different colors corresponded to different values of w, where v = –0.0454. The elliptical outline of the spots distribution stretches along the y-axis as w increases and there is a special position (marked with red dots) where a round spot

Optics EXPRESS

distribution is obtained. Thus, round spot distributions can be obtained by adjusting the incident direction vector.

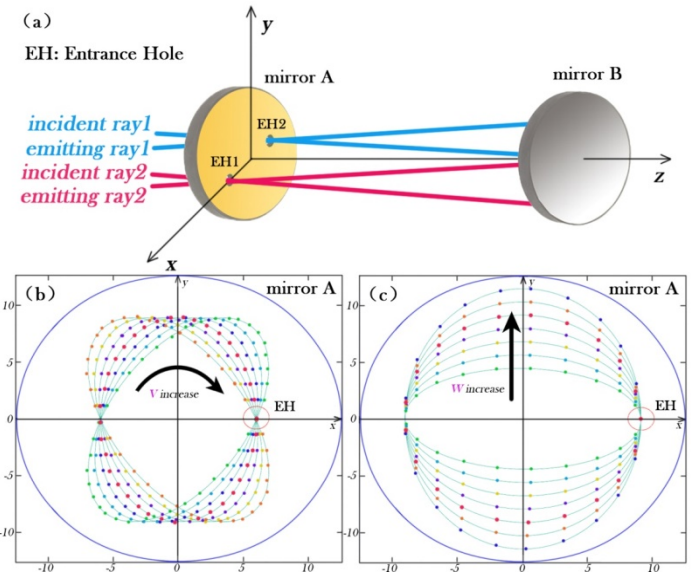

Fig. 1. (a) A generic model of a dual spot-ring Herriott cell (DSR-HC) with two entrance-holes (EH1, EH2) on mirror A and two rays enter and emit the DSR-HC through the same entrance hole, respectively. (b) Spot distributions on mirror A for different values of the parameter v in the direction vector (1, v, w) of the incident ray. (c) Spot distributions for different values of the parameter w in the direction vector (1, v, w) of the incident ray.

2.2. Development of a DSR-HC

Figure 2(a) shows the photograph of the fabricated DSR-HC with a size of 5.5 cm × 9.2 cm × 32.1 cm. A tilted window was used to avoid interference fringes. Mirror A and mirror B were placed facing each other. Two incident rays enter the cell through the coupling holes on mirror A and exit the cell from the same holes after a certain number of reflections between the mirrors. A gas inlet and outlet were located in front and in the rear of the cell, respectively. A sealing ring was placed on top of the cell. Furthermore, the cell could be sealed when the sealing ring is squeezed to deform as result of the pressure from the lid.

As shown in Fig. 2(b), there are two entrance holes (EH1 & EH2) for the two incident rays on mirror A. The directions of the two incident rays are set to obtain two round spot distributions. The number near the reflected dot marks the reflection order. The even numbers are on mirror A and the odd numbers are on mirror B. For each spot ring, the center of the incident spot is at the center of the entrance hole and the center of the emitting spot is marked with ' + '. The total reflection number is 50, where the 0^{th} reflected spot is the incident dot and the 50^{th} reflected dot is the emitting spot. The outer spot-ring (marked with red spots) corresponds to a longer light path, and in this case the radius of the incident spot is adjusted to be small to ensure that there is no light leakage and emitted light blocking. The long light path is calculated to be 19.78 m by the following equation

$$L = \sum_{i=0}^{N} \sqrt{\left[(x_{i+1} - x_i)^2 + (y_{i+1} - y_i)^2 + (z_{i+1} - z_i)^2 \right]} \quad (1)$$

where (x_i, y_i, z_i) is the coordinate of the reflection point, and N is the total reflection number.

The inner spot-ring (marked with green spots) corresponds to a shorter light path. In this case, there is an overlap between the 22^{nd} reflected spot and the entrance hole (EH2), so partial light within the 22^{nd} reflected spot will emit from the entrance hole (EH2) and reach

Optics EXPRESS

the detector in advance. The residual light has to complete an additional 28 reflections before reaching the detector. So the light reaching the detector consists of 2 components including the leaked light with only 22 reflections and the light with 50 reflections. As the light intensity in the reflected spot obeys a Gaussian distribution, the intensity of the leaked light is the integral within the leaked area. The equivalent light path corresponding to the inner spot-ring is calculated by Eq. (2)

$$L = -\frac{1}{-S\varphi P\chi}\ln\left[k\exp(-S\varphi P\chi L_1) + (1-k)\exp(-S\varphi P\chi L_2)\right] \tag{2}$$

where S is the absorption line intensity, φ is the line shape function, P is the gas pressure, χ is the test gas volume ratio, k is the ratio between the leaked intensity and the total intensity, and L_1 and L_2 are the optical light path length corresponding to the 22 and 50 reflections, respectively. The inner ring possesses a path length of 6.12 m. By using a trace laser, Fig. 2(c) shows the measured spot distribution on mirror A, which is consistent with the results shown in Fig. 2(b).

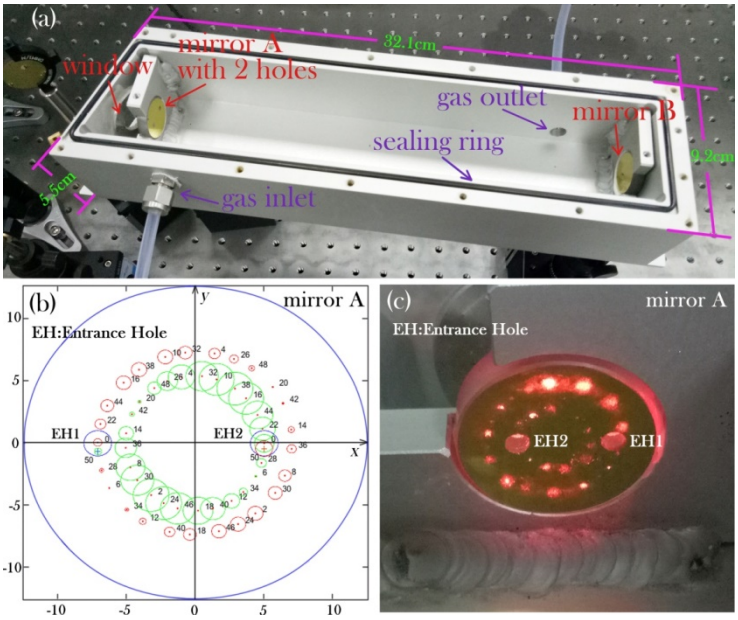

Fig. 2. (a) Photograph of the fabricated DSR-HC with a dimension size of 5.5 cm × 9.2 cm × 32.1 cm. (b) Simulated spot distribution on mirror A, where two entrance holes (EH1 & EH2) for the two incident rays were on mirror A. (c) Observed spot distribution on mirror A.

2.3. Absorption path length determination of the DSR-HC

A saw-tooth wave signal with a frequency of 5 Hz was used to modulate the current of the DFB laser. A C_2H_2 sample with a concentration level of 1000 ppmv was used to rinsing the cell. As shown in Fig. 3(a), the maximum absorption of the detector's response occurred at 53.09 ms and the corresponding voltage (V_1) was 1.18 V. The red line was the fitted background signal. The non-absorption voltage (V_2) on the red line was 1.3 V at a time of 53.09 ms. As the detector had an inherent bias voltage (V_{OFFSET}) which was equal to 0.65 V, the absorbance (α) can be calculated from Eq. (3)

$$\alpha = -\ln((V_2 - V_{OFFSET}) / (V_1 - V_{OFFSET})) \tag{3}$$

Therefore, the absorbance using the inner spots circle was 0.204, corresponding to a light path of 6 m as compared to the simulation result on the SpectraPlot website [26]. In Fig. 3(b), the

Optics EXPRESS

outer circle of the reflected spots was used. As the size of the pinhole became smaller, the amplitude of the signal decreased along with the reduction of the light intensity reaching the detector. According to Eq. (3), the absorption using the outer spots circle was 0.663, resulting in a light path of 20 m. Consequently, two light paths of 6 m and 20 m were obtained in one cell, which were close to the simulated lengths of 6.12 m and 19.78 m.

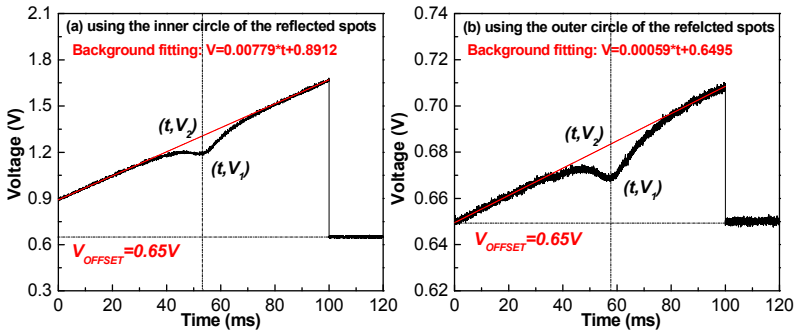

Fig. 3. Measured C_2H_2 absorption signal (black curve) with the reported DSR-HC at a concentration level of 1000 ppmv, (a) using the inner spot ring, and (b) using the outer spot ring. The red curve shows the background fitting signal.

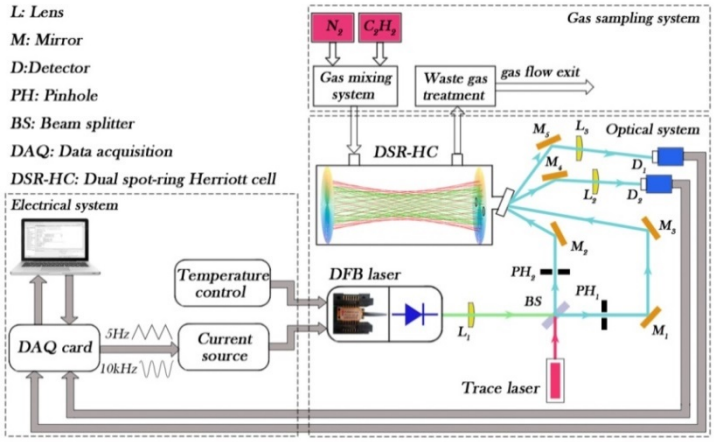

Fig. 4. Double-range C_2H_2 sensor structure using the developed DSR-HC, including an electrical system, an optical system as well as a gas sampling system.

3. C_2H_2 Sensor design using the DSR-HC

3.1. Sensor configuration

The C_2H_2 sensor structure is depicted in Fig. 4, including the electrical, the optical and a gas sampling system. The electrical system consists of a laptop, a data acquisition (DAQ) card (Model USB-6211, National Instrument, USA) and an integrated laser current driver and temperature controller (LDTC0520, Wavelength, USA). The temperature of the DFB laser was set to 23.8 °C. A scan and modulation signal (5 Hz triangular-wave plus a 5 kHz sine-wave) were generated by the LabVIEW controlled DAQ card to drive the DFB laser. The signals from the two detectors (PDA10, Thorlabs, USA) were sent to the DAQ for data acquisition triggered by the signal generation module of the DAQ.

In the optical system, the light from the DFB laser is collimated by lens 1 (L_1), and combined with the light from the trace laser on a beam splitter (BS). Pinholes (PH_1, PH_2) were used to adjust the size of each incident spot. Beam 1 was reflected by mirror 2 (M_2) and beam 2 was reflected by mirrors 1 (M_1) and mirror 3 (M_3). The two beams were injected into

Optics EXPRESS

the DSR-HC through two entrance holes on mirror A. The exit beams from the cell were reflected by mirror 4 and 5 (M_4, M_5), and focused on two detectors (D_1, D_2) through lens 2, 3 (L_2, L_3), respectively.

In the gas sampling system, nitrogen (N_2) was used as the carrier gas to mix with C_2H_2 to obtain gas samples with different concentration levels through a gas mixing system (Series 4000, Environics, USA).

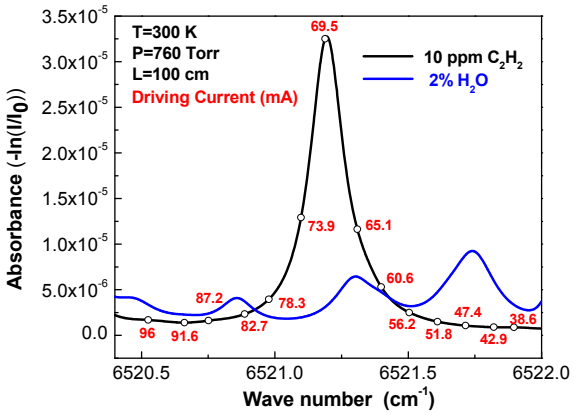

Fig. 5. HITRAN based absorption spectra of C_2H_2 (10 ppmv) and H_2O (2%) in a narrow spectral range from 6520.4 cm^{-1} to 6522 cm^{-1} at a pressure of 760 Torr and an absorption path length of 100 cm. C_2H_2 and H_2O lines are shown in black and blue, respectively. The red number is the driving current required to obtain a corresponding wavenumber marked by round dot.

3.2. C_2H_2 line selection

The selection of the optimum target C_2H_2 absorption line was carried out by a comprehensive survey of the HITRAN database. The C_2H_2 molecule has an overtone vibrational band near 1.53 μm. Figure 5 shows that the transmission spectra of 10 ppmv C_2H_2 and 2% water vapor (H_2O) in the spectral region from 6520.4 to 6522 cm^{-1}. The simulated emission conditions were at a gas pressure of 760 Torr, a temperature of 300 K and an optical path length of 100 cm. The C_2H_2 absorption at 6521.2 cm^{-1} is found to be free from H_2O interference due to a small water vapor absorption. When the temperature of the DFB laser was set to 23.8 °C, the driving currents corresponding to the wavenumbers are marked by round dots on the absorption curve, which was measured with a Fourier Transform Infrared Spectrometer (FTIR, Thermo Fisher Scientific, model Nicolet Is50 FT-IR).The scan range of the driving current was set to 38–96 mA, corresponding to a wavenumber range of 6520.4–6522 cm^{-1}.

3.3. Modulation depth optimization

In order to optimize the detection sensitivity of the C_2H_2 sensor system, an appropriate choice of the modulation amplitude was required to maximize the 2*f* signal amplitude. The optimum modulation depth is 2.2 times of the half width at half maximum (HWHM) of the absorption line [27], which was ~0.187 cm^{-1}. This requires an amplitude of the modulation current of 7.8 mA according to the relationship between the laser driving current and the laser emission wavenumber (0.024 cm^{-1}/mA). Then the theoretical amplitude of the modulation signal was calculated to be 31 mV based on the I/V relation of the laser driver (3.977 mA/V). The amplitudes of the C_2H_2 2*f*-signals were recorded for different modulation amplitudes as plotted in Fig. 6, where the C_2H_2 concentration level was 1000 ppmv. The 2*f* signal amplitude continues to increase with the modulation amplitude without finding the maximum value. Considering the allowed maximum laser driving current and the maximum modulation

Optics EXPRESS

current (should be smaller than the scan current), a modulation amplitude of 40 mV was selected.

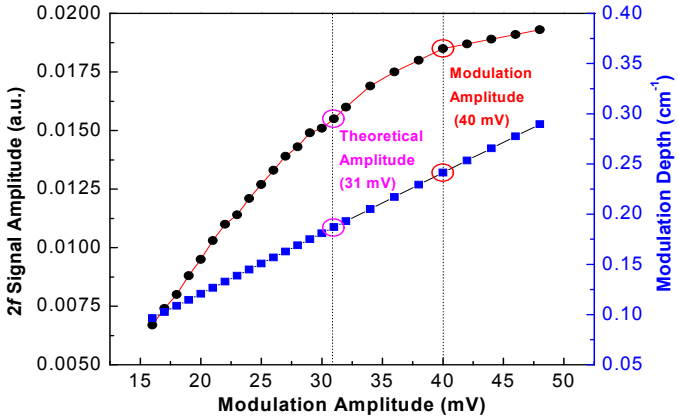

Fig. 6. Modulation depth and the C_2H_2 2*f*-signal amplitude as a function of the modulation amplitude of the sinewave signal.

4. C_2H_2 sensor performances with a DSR-HC

4.1. Experimental details

For targeting the C_2H_2 absorption line at 6521.2 cm^{-1}, the DFB laser drive current and temperature were set to 67 mA and 23.8 °C, respectively. The scan signal was a triangular signal with a frequency of 5 Hz and a peak-to-peak amplitude of 0.26 V. The sine-wave modulation signal possessed a frequency of 5 kHz and a peak-to-peak amplitude of 40 mV. The sampling rate of the ADC module in the DAQ card was set to 100 kHz, resulting in 20,000 data points per triangular period. Sync sampling was realized by using the scan signal of the laser as a trigger signal. Data sampling and processing were realized on a LabVIEW based platform.

4.2. Sensor performances with the 20 m cell configuration

4.2.1 Calibration and data-fitting

The outer spot ring corresponding to a long light path (20 m) was used for the calibration of low-concentration C_2H_2 measurements. The C_2H_2 gas samples in the range of 10 to100 ppmv in steps of 10 ppmv concentration levels were prepared using the gas mixing system. The 2*f* signal was acquired, by means of a lock-in amplifier program based on LabVIEW. The 2*f* amplitude was recorded for ~5 min for each C_2H_2concentration level, as shown in Fig. 7(a). The measured amplitude for each concentration was averaged and plotted as a function of C_2H_2 concentration, as shown in Fig. 7(b). A linear relation was observed between the 2*f* amplitude (2*f*-amp) and the concentration (*C*), given by:

$$C = 0.6382 \times 2f - \text{amp} - 1.2319 \quad (4)$$

The fitting curve indicates a linear relationship (R-square value: 98.87%) between the 2*f* amplitude and C_2H_2 concentration.

Optics EXPRESS

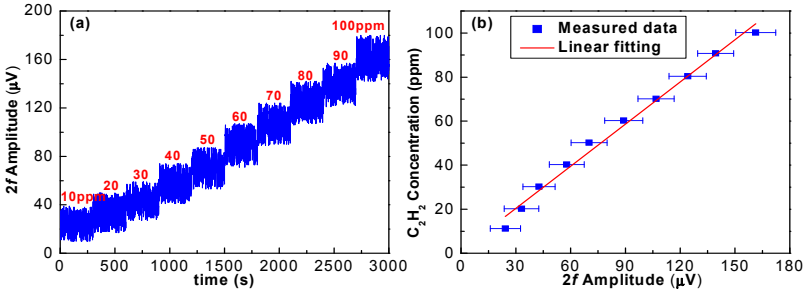

Fig. 7. (a) Measured 2*f* signal amplitude versus calibration time *t* for different C_2H_2 concentration levels ranging from 10 to 100 ppmv. (b) Experimental data dots and fitting curve of C_2H_2 concentration versus the 2*f* signal amplitude.

4.2.2 Sensor stability

The noise level of the C_2H_2 sensor system was determined by passing pure N_2 into the gas cell and the subsequent monitoring of the 2*f* signal. The absorbance was transformed to C_2H_2 concentration levels based on their relationship shown in Eq. (4). Measurements of the C_2H_2 sample with zero concentration were performed over a time period of ~2 hours with a sampling interval of 2 s as shown in Fig. 8. In Fig. 8(a), the total variation range of the measured concentration is ~−8 to −18 ppmv for a 2 hours' observation time. In Fig. 8(b), the Allan deviation was plotted on a log-log scale versus the averaging time, τ. The plot indicates a measurement precision of ~4.0 ppmv with a ~2 s averaging time. A measurement precision of ~0.5 ppmv with a ~100 s averaging time was obtained. The variation trend of the Allan plot indicates a White–Gaussian noise dominated sensor operation.

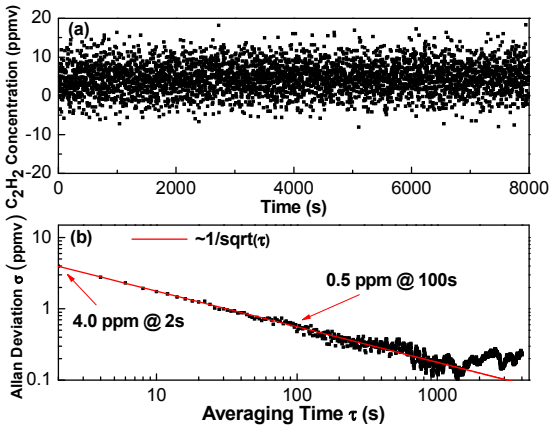

Fig. 8. (a) C_2H_2 concentration measurements of the sample with zero concentration for a time period of ~2 hours using the long light path. (b) Allan deviation plot of the C_2H_2 sensor with a sampling interval of 2 s based on the data shown in Fig. 8(a).

4.3. Sensor performances with a 6 m cell configuration

4.3.1 Calibration and data-fitting

The inner spot ring corresponding to a short light path (6 m) was used in the calibration experiment for high-concentration C_2H_2 measurements. The C_2H_2 gas samples in the range of 100 to1000 ppmv with concentration levels in steps of 100 ppmv were prepared. Taking the same sampling and data processing procedures used in Section 4.2, the measured 2*f* amplitude versus calibration time for different C_2H_2 concentration levels within the 100-1000 ppmv

Optics EXPRESS

range is shown in Fig. 9(a). The averaged measured 2*f* amplitude for each concentration is plotted in Fig. 9(b) with a linear relation given by:

$$C = 104.062 \times 2f - amp - 24.452 \quad (5)$$

The fitting curve indicates a good linear relationship (R-square value: 99.85%) between the 2*f* amplitude and the C_2H_2 concentration levels.

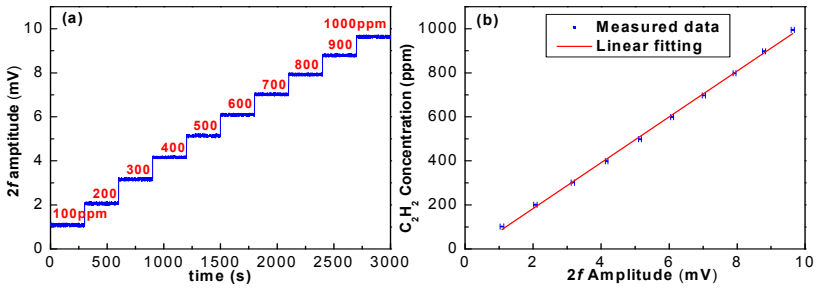

Fig. 9. (a) Measured 2f amplitude versus calibration time t for different C_2H_2 concentration levels within 100-1000 ppmv. (b) Experimental data dots and fitting curve of C_2H_2 concentration versus the 2*f* signal amplitude.

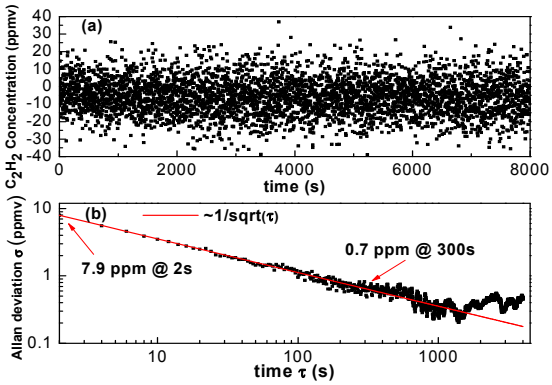

Fig. 10. (a) C_2H_2 concentration measurements of the sample with zero concentration over a time period of ~2 hours using the short light path. (b) Allan deviation plot of the C_2H_2 sensor with a sampling interval of 2 s based on the data shown in Fig. 10 (b).

4.3.2 Sensor stability

Similarly, C_2H_2 concentration measurements of the sample with zero concentration were performed over a time period of ~2 hours with a sampling interval of 2 s. As shown in Fig. 10(a), the total variation range of the measured concentration is ~–40–39 ppmv. As shown by the Allan deviation plot in Fig. 10(b), the result indicates a measurement precision of ~7.9 ppmv with a ~2 s averaging time and a measurement precision of ~0.7 ppmv with a ~300 s averaging time.

4.4 Comparison

The simulated absorbance is shown in Table 1 based on the HITRAN database, according to the experimental conditions, i.e., a temperature of 300 K and a pressure of 760 Torr. Using the outer spots circle with a 20 m light path length, the achieved absorbance is 0.0026 when the 1σ limit of detection (LoD) is 4.0 ppmv. Using the inner spots circle with a 6 m light path length, the absorbance is 0.0016 when the 1σ LoD is 7.9 ppmv. As the theoretical detection limit of the absorbance based on the tunable diode laser absorption spectroscopy (TDLAS)

Optics EXPRESS

technology is ~0.001, the measured absorbance is close to the theoretical limit which illustrates good performance of the C_2H_2 sensor system.

Table 1. Simulated absorbance corresponding to 20 m and 6 m absorption path length when the temperature is set to 300K and the pressure is set to 760 Torr.

Absorption path length (m)	1σ LoD (ppmv)	Absorbance
20	4.0	0.0026
6	7.9	0.0016

If a long absorption path is required, more reflections are required in the cell, which causes a greater loss of the received light intensity due to the limited reflectivity of the mirror compared with the case using a short absorption path. The quantization noise cannot be ignored when the detector signal is in μV level range, which is close to the ADC resolution of the DAQ card when a 20 m light path was used. As the detector signal is at the mV level when a 6 m light path was used, the signal-to-noise ratio (SNR) with a short light path is higher than that with a long light path, which will make the absorbance with a 6 m light path (0.0016) closer to the theoretical limit (0.001) than that with a 20 m path length (0.0026). Furthermore, although the absorption path length is three times longer, the 1σ LoD for a 20 m path length is not three times smaller than that for the LoD of a 6 m optical path length.

4.5 Disadvantages of the DSR-HC

The design of the proposed DSR-HC requires a careful calculation and simulation of the two rings and each spot size, which differs from a traditional Herriott cell with only one spot-ring. Furthermore, the DSR-HC has two entrance holes for light injection. So there is a need for more optics to inject two light beams into the cell and also to reflect the two exit beams into detectors. This increases the overall complexity of the optical platform. Besides, a careful adjust on the two mirror positions as well as the direction of the two incident beams is required for beam alignment, which is also complicated due to more steps for aligning the two beams.

5. Conclusions

Modeling and fabrication of a novel DSR-HC were presented, which improves the utilization efficiency of the Herriott mirror by generating more reflected spots on the surface. A C_2H_2 sensor system was developed using the DSR-HC with two absorption lengths of ~20 m and ~6 m, respectively, by dividing the laser beam into two parts and injecting the two beams simultaneously into the DSR-HC. Experiments were carried out to validate the operation of the DSR-HC and derive the performances of the sensor system using diluted C_2H_2 samples. An Allan-Werle deviation analysis was carried out for the sensor system using the two absorption lengths, respectively. Though the design, fabrication and alignment of the DSR-HC are complicated compared to a traditional Herriott cell with one spot-ring, the DSR-HC is capable of single-gas detection with two different measurement ranges and also dual-gas detection with different absorption lengths. Therefore, the proposed DSR-HC expands the application of a Herriott cell in the field of gas sensing based on infrared absorption spectroscopy.

Funding

National Natural Science Foundation of China (Nos. 61775079, 61627823, 61307124); National Key R & D Program of China (Nos. 2016YFD0700101, 2016YFC0303902, 2017YFB0402800); Key Science and Technology "R & D" Program of Jilin Province, China (No. 20180201046GX); Science and Technology Planning Project of Guangdong Province, China (No. 2017A020216011); Industrial Innovation Program of Jilin Province, China (No. 2017C027); National Science Foundation (NSF) ERC MIRTHE award; Robert Welch Foundation (No. R4925U).

168.7.248.130 {ts '2019-01-18 15:53:59'}